The influence of the austenite grain size on the microstructural development during quenching and partitioning processing of a low-carbon steel

Celada-Casero, Carola; Kwakernaak, Cees; Sietsma, Jilt; Santofimia, Maria Jesus

DOI
10.1016/j.matdes.2019.107847

Publication date
2019

Document Version
Final published version

Published in
Materials and Design

Materials and Design 178 (2019) 107847

Contents lists available at ScienceDirect

Materials and Design

journal homepage: www.elsevier.com/locate/matdes

The influence of the austenite grain size on the microstructural development during quenching and partitioning processing of a low-carbon steel

Carola Celada-Casero *, Cees Kwakernaak, Jilt Sietsma, Maria Jesus Santofimia

Department of Materials Science and Engineering, Delft University of Technology, Mekelweg 2, 2628CD Delft, the Netherlands

HIGHLIGHTS

- Under fixed Q&P conditions, the PAGS influences the phase fractions and retained austenite stability of the final microstructure
- Small-grained microstructures promote a more efficient carbon partitioning process than coarser microstructures
- For the investigated partitioning conditions and PAGSs, there is a linear dependency between the primary and fresh martensite fractions
- The PAGS renders an optimum fraction of primary martensite that minimises fresh martensite and stabilizes sufficient austenite

GRAPHICAL ABSTRACT

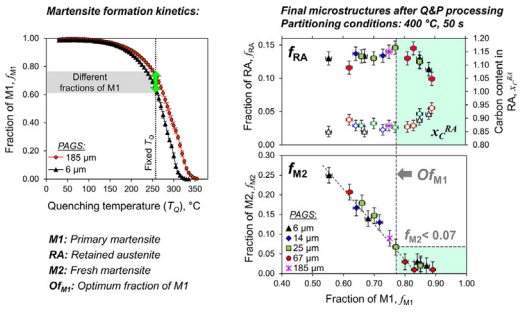

ARTICLE INFO

Article history:
Received 28 February 2019
Received in revised form 8 May 2019
Accepted 10 May 2019
Available online 17 May 2019

Keywords:
Prior austenite grain size
Microstructural design
Martensite
Retained austenite
Carbon partitioning
Quenching & Partitioning

ABSTRACT

The influence of the prior austenite grain size (PAGS), varying between 6 and 185 μm, on the microstructural development of a low carbon steel during quenching and partitioning (Q&P) processing is investigated. The effect on the size and morphological aspects of the microconstituents is discussed based on the kinetics of carbon redistribution between martensite and austenite upon partitioning conditions of 400 °C and 50 s. Under fixed quenching and partitioning conditions, decreasing the PAGS leads to a more efficient carbon partitioning process through the smaller and more homogeneously distributed phases developed during the first quench. In contrast, the microstructural heterogeneity obtained with larger PAGSs makes it more difficult to control the degree of carbon enrichment in austenite during partitioning and thus the austenite stability. Additionally, large volumes of fresh martensite are more likely to form in the interior of large-scale austenite grains due to the incomplete carbon homogenisation process. To consider the PAGS in the design of Q&P microstructures the selection of an optimum fraction of primary martensite is proposed, which ensures the minimisation of fresh martensite in the final microstructure and the sufficient stabilisation of the austenite phase. This new methodology facilitates the applicability of the Q&P process providing a controlled and reproducible development of optimised Q&P microstructures.

1. Introduction

Optimisation and adjustment of properties to a certain application in advanced steels can only be performed through accurate

* Corresponding author.
E-mail addresses: C.CeladaCasero@tudelft.nl (C. Celada-Casero), C.Kwakernaak@tudelft.nl (C. Kwakernaak), J.Sietsma@tudelft.nl (J. Sietsma), M.J.SantofimiaNavarro@tudelft.nl (M.J. Santofimia).

https://doi.org/10.1016/j.matdes.2019.107847

microstructural design. The development of the third generation of Advanced High-Strength Steels (AHSS), as termed for automotive applications [1], relies on the design of microstructures consisting of high strength phases, such as martensite, bainite or ultra-fine ferrite, and a significant fraction of soft and ductile constituents, as ferrite and austenite [2,3]. Such microstructural combination results in increasing strength-ductility levels. The quenching and partitioning (Q&P) cycle proposed by Speer [4–6], has been demonstrated to be very promising for the development of such AHSSs. For instance, de Moor and co-authors [7] measured by tensile testing strengths of 1500 MPa with total elongations of 15% in a 0.3C-3Mn-1.6Si (wt%) steel.

If the aim is to create microstructures formed by martensite and retained austenite, the Q&P process starts with the full austenitisation of the steel. Then, the material is quenched to a temperature between the martensite start temperature (M_S) and room temperature to form a controlled fraction of primary martensite (M1). Subsequently, the steel is subjected to a partitioning treatment to promote the diffusion of carbon from the supersaturated martensite to the untransformed austenite. This stage aims at the stabilisation of the austenite phase at room temperature. However, carbon competing reactions, such as carbides precipitation in M1 or bainite formation, may occur even in carefully designed steels compositions, reducing the fraction of austenite in the final microstructure [8–10]. Additionally, the martensite-austenite interface becomes mobile under some conditions, which may further affect the volume fractions of phases and austenite carbon content, as modelled by Santofimia et al. [11,12]. These processes cause deviations between theoretical calculations based on full carbon partitioning and experimental observations, which hampers the accurate prediction of the Q&P microstructural development.

Grain refinement has been proven to be a powerful strengthening strategy in different microstructural design concepts since it allows the controlled creation of boundaries to obstruct dislocation motion. Q&P processing routes might also benefit from prior austenite grain refinement. Cho et al. [13] showed that the refinement of the Q&P microstructure when the prior austenite grain size (PAGS) is decreased from 6 to 4.4 μm in medium-Mn Q&P microstructures leads to augmented strength above 1500 MPa while sustaining total elongation of 21%. In addition to the improvement of mechanical properties, it was suggested that microstructures of smaller scale result in a faster carbon redistribution during the partitioning stage. However, as highlighted by Speer and co-authors in their "critical assessment for quenching and partitioning" [14], changes in the PAGS would affect the martensite start temperature and, therefore, the prediction of Q&P phase fractions. How the austenite grain structure might affect the evolution of phases, their size and morphology and the kinetics of carbon partitioning is still an unresolved issue to date.

This work aims to understand the influence of austenitisation conditions, through the prior austenite grain size, on the microstructural development during quenching and partitioning including size and morphological changes of microconstituents as well as the kinetics of carbon redistribution between martensite and austenite. The outcomes from this research will enable to improve the methodologies for the design of controlled and reproducible Q&P processing routes facilitating their applicability.

2. Experimental procedure

2.1. Material and microstructural design

A hot-rolled low-carbon steel with Mn and Si contents usual in Q&P steels is investigated (0.2C-3.5Mn-1.5Si, in wt%). The steel exhibits starting-finishing austenitisation temperatures (A_{C1} – A_{C3}) of 720 and 880 °C upon a heating rate of 5 °C/s. Cylindrical samples of 10 mm in length and 3.5 mm in diameter were machined parallel to the rolling direction and heat treated under vacuum in a Bähr DIL 805A/D dilatometer. Five different PAGSs of 185, 67, 25, 14 and 6 μm (±1 μm) were created by varying the austenitisation temperature (T_γ) between 900 and 1200 °C in intervals of 100 °C (Fig. 1a) and by thermal cycling [15] after austenitisation at 900 °C (Fig. 1b), as detailed in a previous work [16]. After reaching the target austenite grain size the specimens were quenched at 50 °C/s to different quenching temperatures (T_Q) (Table 1) and then subjected to a typical partitioning treatment: isothermal holding at a partitioning temperature (T_P) of 400 °C for 50 s. This partitioning time is long enough for a considerable partitioning of carbon from martensite to austenite, and short enough to avoid significant tempering of the martensite [2,9,17]. Finally, the specimens were cooled to room temperature at 20 °C/s. The specimens are referred to as Q&P–PAGS, being PAGS a number in the range of 6 to 185. The martensitic transformation was characterised using additional as-quenched specimens (as-Q), created by direct quench at 50 °C/s to room temperature from the austenitisation conditions.

2.2. Characterisation methods

The Q&P specimens were prepared for microstructural characterisation by grinding, polishing down to 1 μm and etching with 2% Nital for 5 s. Scanning electron microscopy (SEM) and electron backscatter diffraction (EBSD) were performed using a JEOL JSM-6500F scanning electron microscope (SEM) operating at 15 kV. A final polishing step with 0.05 μm OPS suspension for 15 min was included for EBSD analysis. Data acquisition was performed with an acceleration voltage of 20 kV, working distance of 25 mm and step size of 50 nm. Several areas of 30 μm × 30 μm were scanned for each condition. The post-processing was done using Channel 5 software (Oxford Instruments). Inverse Pole Figure (IPF) maps of bcc and fcc phases were obtained for selected Q&P microstructures. Martensite blocks were defined as bcc phase

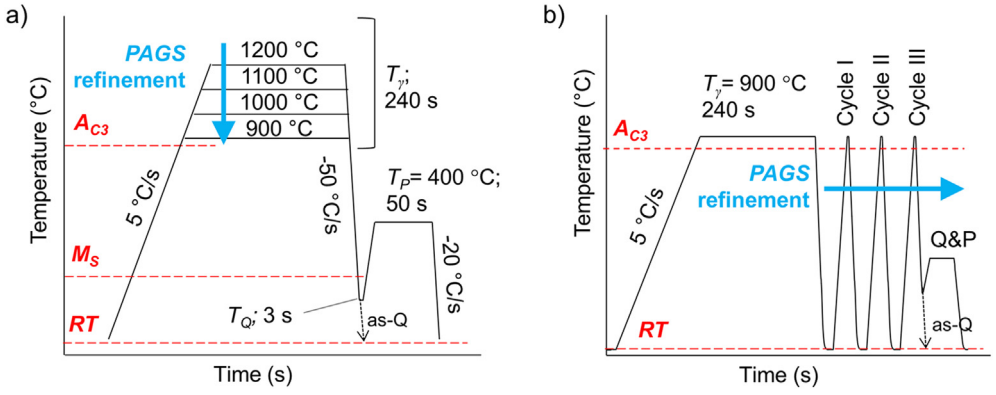

Fig. 1. Schematic representation of the Q&P thermal cycles: (a) the austenitisation temperature (T_γ) is varied between 900 and 1200 °C to vary the PAGS between 14 and 185 μm; (b) thermal cycling is included after austenitisation at 900 °C to create the specimen with a PAGS of 6 μm.

Table 1
Summary of quenching temperatures (T_Q) used to create Q&P microstructures from different prior austenite grain sizes (PAGS).

		PAGS, μm				
		6	14	25	67	185
T_Q, °C	215	✓				
	225	✓	✓	✓	✓	
	250				✓	
	260	✓	✓	✓	✓	✓
	270			✓		
	285	✓	✓	✓	✓	

outlined by high angle grain boundaries (HAGBs), which have misorientations larger than 15°. The retained austenite phase was characterised as fcc phase.

The size and morphology of martensite blocks and retained austenite grains were studied based on the area, the length and the width of the features as defined in the IPF maps. The aspect ratio (φ) of the features is defined as the feature length (l) over the width (w). The martensite lath width was measured using misorientation profile lines drawn perpendicular to the expected lath habit plane in multiple martensite blocks and considering misorientations lower than 3° [18].

X-ray diffraction (XRD) scans in the 2θ range 40°–130° using a step size of 0.035° and a counting time per step of 2 s were performed using Co Kα radiation in a Bruker type d8-Advance diffractometer equipped with a Vantec position sensitive detector. The 2θ range used covers the {110}α, {200}α, {211}α {220}α and the {111}γ, {200}γ, {220}γ and {311}γ reflections. Rietveld refinement of diffractograms and data evaluation was done using the Bruker software DIFFRAC.EVA 4.2.2. The volume fraction of retained austenite was determined by direct comparison of the aforementioned austenite and martensite peaks was used as described by Jatczak [19]. The lattice parameter of the retained austenite was calculated following the Nelson-Riley method [20], from which its carbon content (x_c^{RA}) can be determined from [21]:

$$a_\gamma = 3.556 + 0.0453x_c^{RA} + 0.00095x_{Mn} + 0.0056x_{Al} \quad (1)$$

where x_i indicates content of alloying element i in phase austenite in wt % and the lattice parameter a_γ is in Ångström.

The volume fraction of primary martensite (f_{M1}) formed at the quenching temperature was calculated applying the lever rule to the as-Q dilatometry curves and using the non-linear thermal expansion behaviour of the fcc and bcc lattices proposed by van Bohemen et al. [22]. The volume fraction of fresh martensite (f_{M2}) was obtained by applying the lever rule to the change in length at room temperature and comparing it with the total change in length of the as-Q specimens. The volume fraction of bainite (f_B) was obtained by balancing the fraction of phases as $f_B = 1 - f_{M1} - f_{RA} - f_{M2}$.

3. Results

3.1. Evolution of phase fractions during the Q&P thermal treatment

Fig. 2a shows the dilatometry curves obtained during the application of Q&P heat treatment in microstructures with PAGSs of 6 μm and 67 μm quenched to $T_Q = 225$ °C. The corresponding as-Q curves are drawn in solid black lines for comparison. Dashed lines represent the extrapolated thermal expansion behaviour of the bcc and fcc lattices as well as of the Q&P microstructures after partitioning, which consist of a mixture of bcc and fcc phases.

The evolution of Q&P phase fractions is analysed based on the three main stages of a Q&P thermal treatment:

1) First quench to the quenching temperature from austenitisation conditions
2) Partitioning stage
3) Final cooling to room temperature

1) During the first quench to $T_Q = 225$ °C, the austenite partially transforms into primary martensite (M1). It is observed in Fig. 2a that the microstructure with the smallest PAGS (Q&P–6 μm) exhibits a lower martensite start temperature (M_S) than the microstructure with the largest PAGS (Q&P–67 μm). Fig. 2b shows the evolution of the volume fraction of primary martensite (f_{M1}) with temperature obtained from the as-Q dilatometry curves. The microstructure with the smallest PAGS has a lower M_S and thus the whole martensite formation kinetics is shifted to lower temperatures with respect to that of the largest PAGS. Therefore, quenching to the same temperature results in lower fractions of M1 for Q&P–6 μm than for Q&P–67 μm, as highlighted in Fig. 2b [16]. Since the kinetic curves converge as the temperature decreases, more similar M1 fractions are obtained with decreasing quenching temperatures.

2) After the first quench, the material is reheated to the partitioning temperature of $T_P = 400$ °C and held for 50 s. In this stage, the carbon of the supersaturated martensite diffuses into the austenite. This increases the thermal stability of the austenite and makes its retention at room temperature possible. Fig. 3 shows the volume fraction (f_{RA}) and carbon content (x_C^{RA}) of retained austenite of final Q&P–6 μm and Q&P–67 μm microstructures as a function of the quenching temperature. A maximum fraction is observed for Q&P–67 μm, whereas Q&P–6 μm exhibits a plateau of maximum fraction over a range of quenching temperatures.

Fig. 4 shows the dilatometry curves during the thermal cycles of Q&P–6 μm and Q&P–67 μm microstructures. The expansion detected

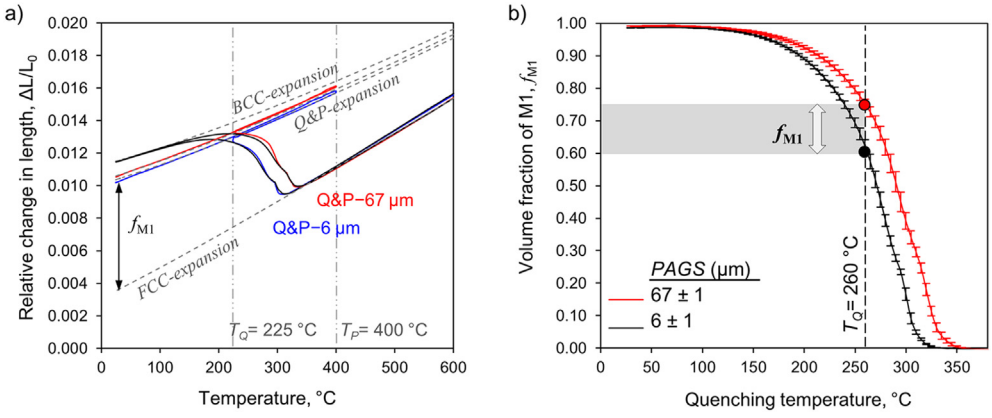

Fig. 2. (a) Dilatometry curves during Q&P cycle of microstructures with PAGS of 6 and 67 μm. The quenching ($T_Q = 225$ °C) and partitioning ($T_P = 400$ °C) temperatures are indicated with vertical dashed lines. Solid blacklines represent the corresponding as-Q curves. (b) Evolution of the volume fraction of primary martensite (M1) with the quenching temperature.

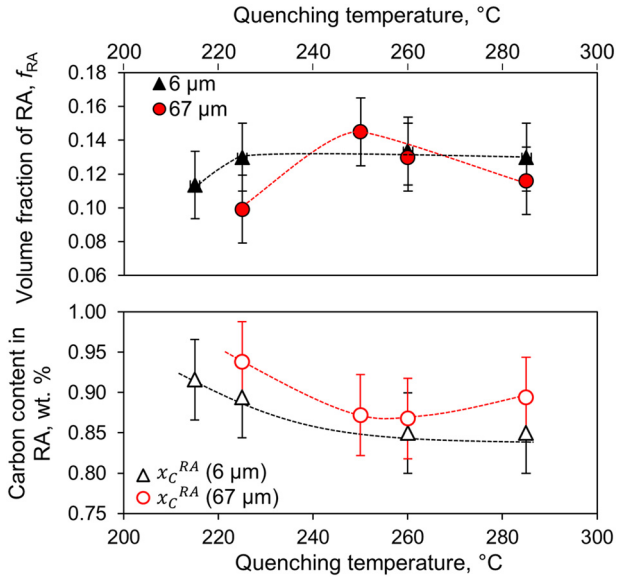

Fig. 3. Volume fraction and carbon content of retained austenite as a function of the quenching temperature for microstructures with a PAGS of 6 and 67 μm. Dashed lines are drawn as a guide to the eye.

at the partitioning temperature (of about 0.03% or lower) can be attributed to the sole austenite volume expansion due to carbon enrichment [23]. This dilatometry behaviour indicates that the phase fractions do not change during the partitioning stage in any of the Q&P conditions. Under conditions of full carbon partitioning, suppression of competitive reactions and fixed martensite/austenite interface [5], the highest fraction of RA is obtained when the total fraction of carbon in M1 is sufficient to ensure the minimum carbon content in the untransformed austenite for its complete stabilisation at room temperature. The corresponding fraction of M1 and austenite phases are achieved at the so-called optimum quenching temperature (OT_Q) [5]. Therefore, microstructures quenched below the OT_Q form high M1 fractions providing carbon to the austenite that exceeds the total carbon fraction required to completely stabilise the untransformed austenite. This results in smaller fractions of RA with increasing carbon contents. In turn, microstructures quenched above the OT_Q form lower M1 fractions whose total carbon fraction is not sufficient to completely stabilise the untransformed austenite. Therefore, the fraction of RA decreases with higher quenching temperatures. This approach seems to explain the trends observed in Fig. 3 for Q&P–67 μm microstructures. Instead, the RA fraction of Q&P–6 μm microstructures is quite insensitive to the quenching temperature.

3) During the final cooling to room temperature, fresh martensite (M2) will form from the austenite that is not sufficiently enriched in carbon. The formation of M2 is identified by an expansion during the final quench, as indicated in the dilatometry curve of the Q&P–6 μm microstructure quenched to 285 °C in Fig. 4a. For both austenite grain sizes, the higher the quenching temperature, the larger the change in length during the final quench and, thus, the larger the fraction of fresh martensite. This trend is to be expected since higher quenching temperatures provide lower fractions of M1 and, consequently, lower fractions of carbon to diffuse into larger fractions of untransformed austenite during the partitioning step. Under the investigated partitioning conditions (400 °C, 50 s) the formation of M2 is suppressed in Q&P–6 μm microstructures to lower quenching temperatures than in Q&P–67 μm.

3.2. Characterisation of Q&P microstructures

Fig. 5 displays EBSD Inverse Pole Figure (IPF) maps of microstructures Q&P–6 μm, created by quenching to 225 °C, and microstructures Q&P–14 μm, Q&P–25 μm and Q&P–67 μm, created by quenching to 260 °C. All microstructures consist of a mixture of retained austenite (f_{RA} ~ 0.13), primary martensite (f_{M1} ~ 0.75–0.85) and some fresh martensite (f_{M2} < 0.10). Left and right columns display the IPF maps of bcc (martensite) and fcc (austenite) phases, respectively. Some prior austenite grain boundaries have been outlined by dotted lines.

The colours on the martensite IPF maps (left column, Fig. 5) show specific crystallographic orientations of this phase, whereas the austenite phase appears coloured in white. The high angle grain boundaries (HAGBs), with misorientations larger than 15°, are drawn in white. In this way blocks of martensite have been identified. The boundaries between austenite and martensite are outlined in black when there is a Kurdjumov-Sachs (KS) orientation relationship. This occurs when the retained austenite grain belongs to the prior austenite grain from which the neighbouring martensite has formed.

The austenite IPF maps (right column, Fig. 5) show the location and distribution of the austenite phase more clearly. Austenite grains are coloured according to their crystallographic orientation. Grains of the same colour exhibit the same crystallographic orientation and thus belong to the same prior austenite grain. Austenite/martensite grain boundaries are outlined in black when there is a KS orientation relation between them and in green for larger misorientations, as it the case of

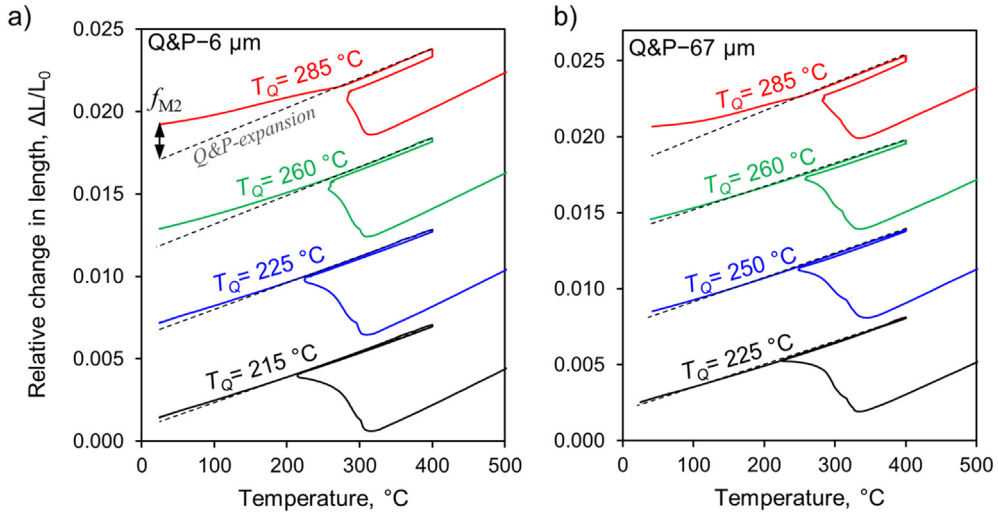

Fig. 4. Dilatometry curves during Q&P cycles of microstructures with PAGS of 6 μm (a) and 67 μm (b). Dashed lines represent the extrapolated expansion behaviour of a Q&P microstructure.

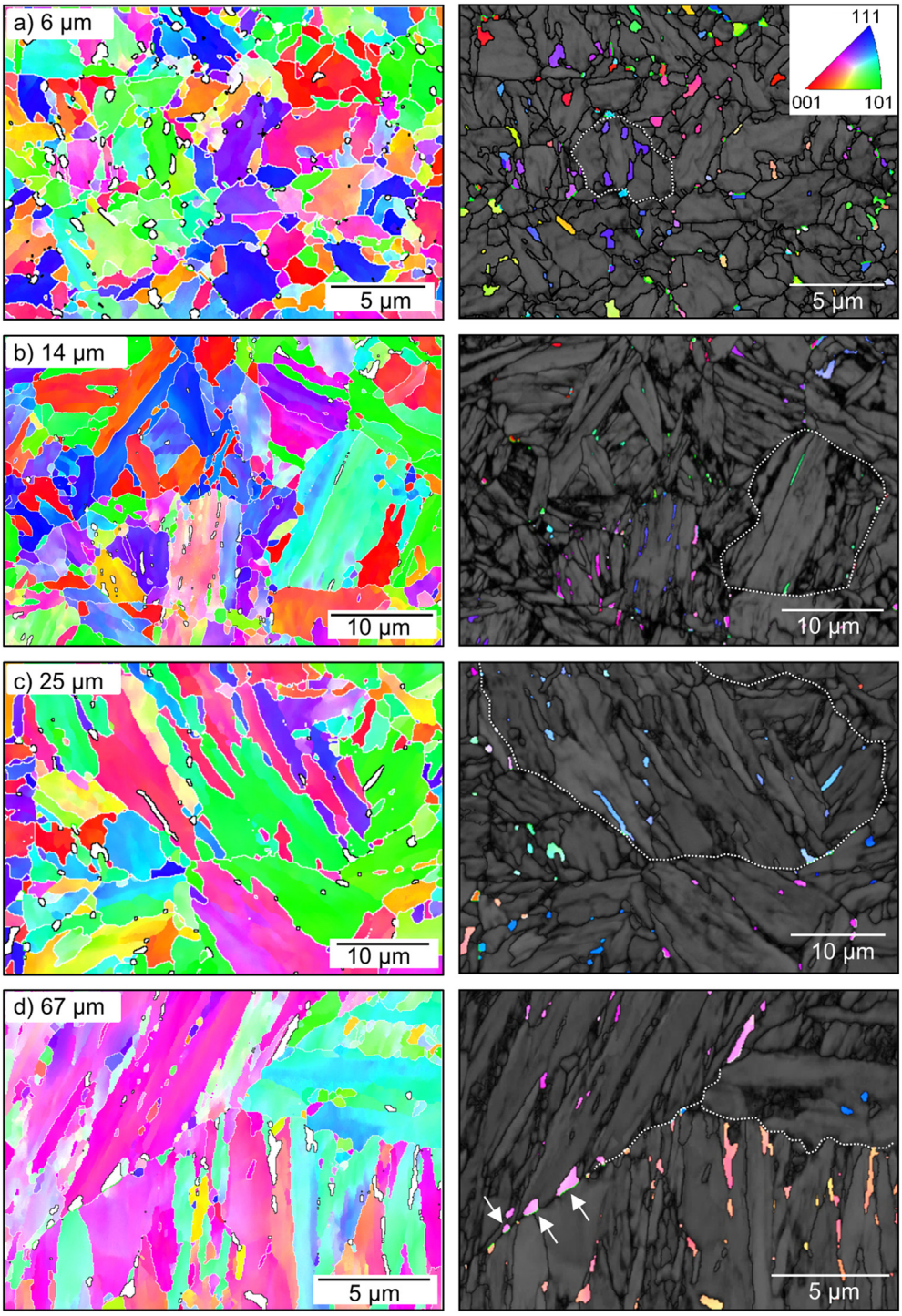

Fig. 5. EBSD IPF maps of Q&P microstructures created from different PAGS as labelled and by quenching to: (a) 225 °C; and (b)–(d) 260 °C. The left- and right-hand side columns display the IPF maps of bcc and fcc phases, respectively. The grey scale in the right-hand side column indicates the image quality of the bcc phase (darker grey signifies lower image quality). The dotted lines outline some prior austenite grain boundaries.

austenite grains located next to a prior austenite grain boundary, as indicated by arrows in Fig. 5d.

The fcc IPF maps are combined with the Image Quality (IQ) map, which displays the martensite phase in different shades of grey and where the martensite/martensite HAGBs are drawn in black. As observed by Santofimia et al. [2,24], lighter areas, exhibiting a higher IQ, correspond to regions with a lower density of lattice defects, like dislocations. These lighter areas are related to the primary martensite phase, which has undergone carbon depletion and partial recovery of lattice imperfections during the isothermal holding at the partitioning temperature. Instead, darker areas present a lower IQ and correspond to the finer, carbon enriched and untempered fresh martensite formed during the final quench.

Fig. 6 shows an SEM micrograph of the Q&P–185 μm microstructure, quenched to 260 °C. Due to the large microstructural scale, EBSD characterisation was not performed on this microstructure. In the SEM, austenite features are disclosed brighter than martensite laths and blocks. As typical in Q&P microstructures [2], films of retained austenite are observed in between martensite laths, whereas RA blocks are next to prior austenite grain boundaries and packet boundaries. Primary martensite

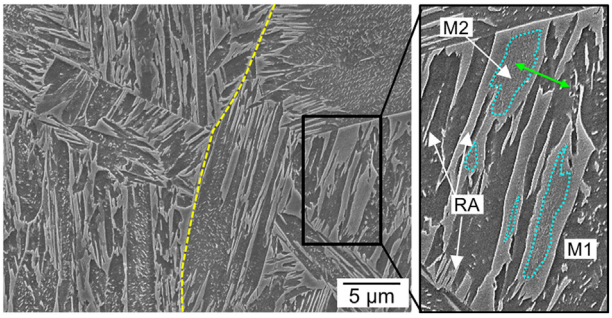

Fig. 6. SEM micrograph of Q&P microstructure created from PAGS – 185 μm by quenching to 260 °C. A prior austenite grain boundary is marked by a dashed yellow line. Dotted lines in the zoomed-in image outline islands of fresh martensite (M2). (For interpretation of the references to colour in this figure legend, the reader is referred to the web version of this article.)

is characterised by the presence of, most likely, transitional carbides that form during the partitioning stage [8].

The zoomed-in image of Fig. 6 reveals that the fresh martensite (enclosed by dotted lines) is located next to or surrounded by retained austenite. It is common to observe rings of RA surrounding islands of M2 when carbon is not homogeneously distributed across the austenite grain during the partitioning stage [24]. This yields higher carbon contents close to the martensite/austenite interface than in the inner part of the austenite grain. The inner part of the grain eventually transforms into fresh martensite during the final cooling [3].

3.3. Distribution, size and morphology of Q&P microconstituents

Fig. 7 shows box and whisker plots of the prior austenite grain size distributions obtained for each austenitisation condition, as characterised in a previous work (see [16]). The top and bottom limits of the boxes and the middle line represent the third and first quartile and the median of the distributions, respectively. The mean PAGS values are displayed as diamond data points. The microstructure with the smallest PAGS (6 μm) exhibits the narrowest distribution, being the mean PAGS value and the median close to each other. This indicates that the distribution is highly symmetric. In contrast, with the increase of the PAGS, the distribution broadens exponentially and the mean values become larger than the median, especially for PAGS larger than 14 μm.

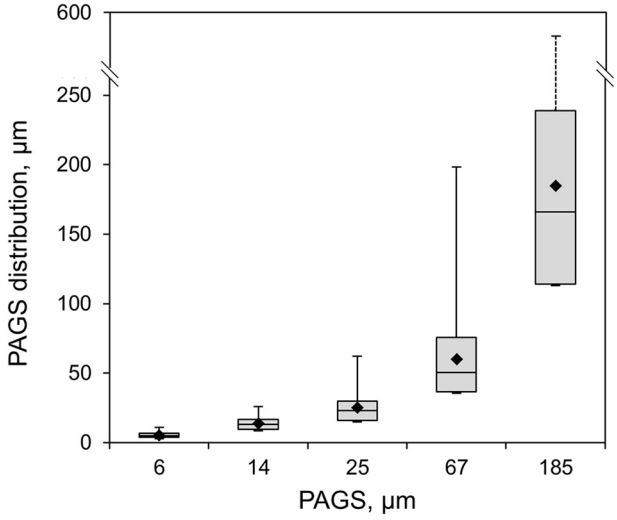

Fig. 7. Box and whisker plots showing the distribution of the prior austenite grain size for the different austenitisation conditions: thermal cycling and austenitisation at 900, 1000, 1100 and 1200 °C.

The influence of the PAGS on the size and morphology of the Q&P microconstituents was investigated based on the area, length, width and aspect ratio of the microstructural features as defined in the IPF maps presented in Fig. 5. The evolution of morphological parameters with the PAGS is presented in Fig. 8 for the primary martensite and the retained austenite phases.

Fig. 8a shows that higher mean values of martensite block length (l_B) and width (w_B) are obtained with increasing PAGS. The increment is more pronounced for prior austenite grain sizes up to 14 μm than for larger PAGSs, particularly for the martensite width. The aspect ratio of the martensite blocks ($\varphi_B = l_B/w_B$) varies linearly with the PAGS.

Fig. 8b represents the length and width distributions of the martensite blocks. Both distribution peaks shift to larger values and broaden with the increase of the PAGS. A similar trend is seen in the distribution of the block aspect ratio presented in Fig. 8c. These results indicate that the martensite blocks created from smaller PAGSs are more homogeneous in size and more equiaxed in morphology than the martensite blocks of microstructures with larger PAGS. This characteristic is also identified in the EBSD maps (Fig. 5) and has been previously noted by other authors [25–28]. On the other hand, the martensite lath width appears to be invariant with the PAGS. An average value of 0.22 ± 0.02 μm was found independently of the PAGS, which agrees well with previous characterisation by transmission electron microscopy in low carbon steels [25,29,30].

The lower part of Fig. 8 shows the characteristics of the grains of retained austenite detected by EBSD. The representation of RA films is significantly underestimated since their thickness might be smaller than the step size used to scan the microstructures by EBSD (50 nm).

Fig. 8d shows that there is an increase of the average grain size (d_{RA}) with the PAGS, being the grain size defined as the diameter of a circle having the same area as the grain. Similarly to the behaviour observed for the martensite block size, RA grain size increases significantly for PAGS below 14 μm and very slightly for larger PAGSs.

Fig. 8e represents the size distribution of the RA grains. Although similar d_{RA} values are obtained for PAGS of 14 μm or larger, the distribution broadens with increasing PAGSs. This indicates that the retained austenite of Q&P microstructures created from PAGS below 14 μm is more homogeneous in size than that obtained from larger PAGSs. The aspect ratio distribution of RA grains (φ_{RA}) is presented in Fig. 8f. The morphology of the RA in the Q&P–6 μm microstructure is mainly elongated, with the length being about twice the width (peak located at $\varphi_{RA} = 2$). Instead, in microstructures created from coarser PAGS the RA exhibits a more equiaxed shape, as the higher representation of frequencies at $\varphi_{RA} = 1$ reveals.

4. Discussion

4.1. Effect of constituents size and morphology on carbon partitioning

To understand the influence of the size and morphology of the austenite on the redistribution of carbon during the partitioning stage, 1D simulations of the local carbon diffusion from the supersaturated martensite to austenite were performed using the Dictra software and the TCFE9 and MOBFE3 databases. A Fe-C-Mn-Si system, with chemical composition similar to the studied alloy, was considered to undergo partitioning at 400 °C. The simulation domain is assumed to be a bicrystal where the martensite and austenite phases are in contact through a planar and fixed interface, as sketched in Fig. 9a. The carbon content of both phases at time $t_P = 0$ s of partitioning is 0.2 wt%. Carbon diffuses from martensite to austenite until its chemical potential is equal in both phases. The diffusion of substitutional elements is considered negligible at this temperature. Mirror boundary conditions are defined at the border of the calculation domains.

The simulation domains were selected as half the martensite block width and half the RA grain size as measured by EBSD (Fig. 8a and e). Experimentally measured phase sizes and fractions of the Q&P

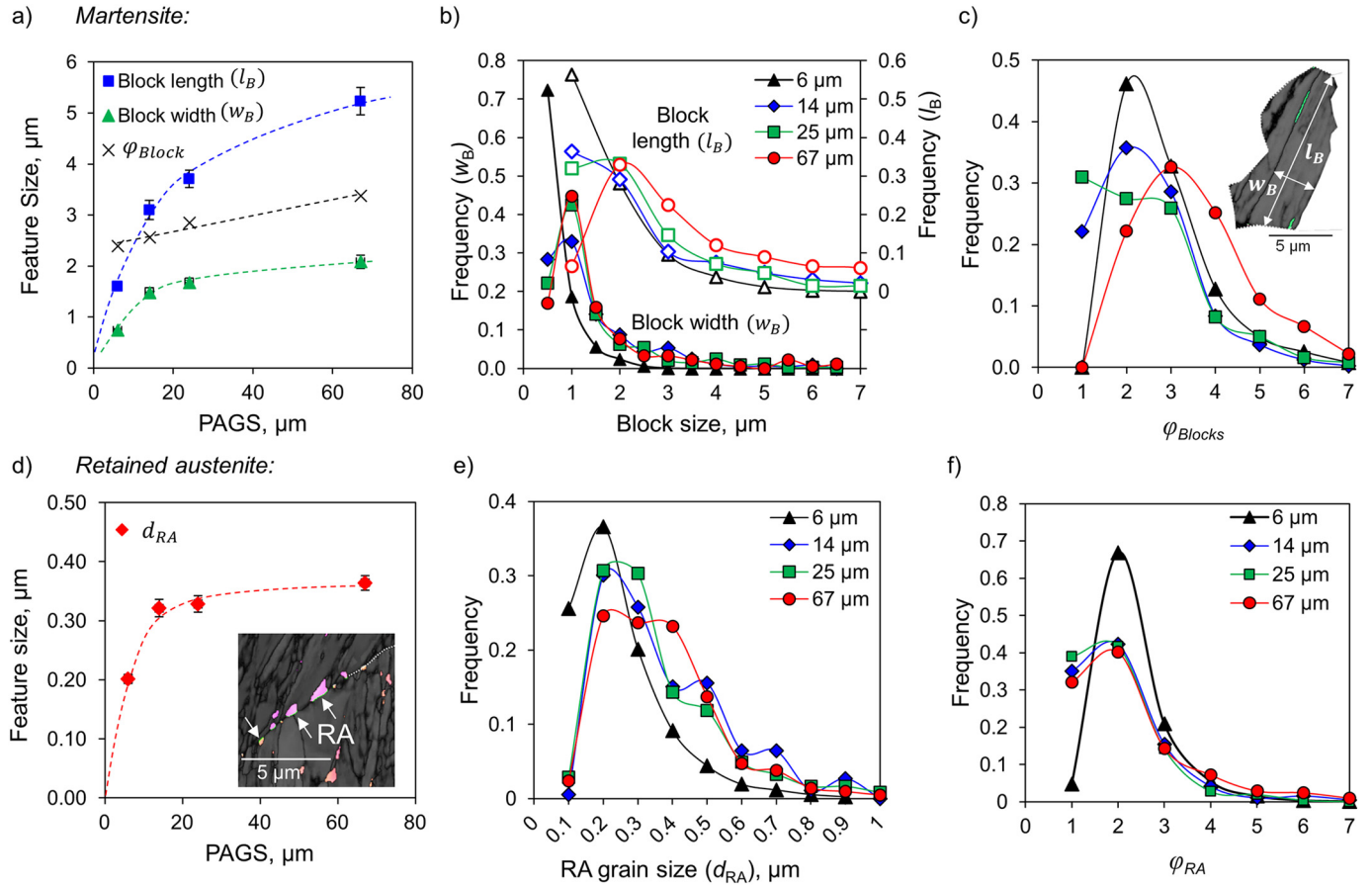

Fig. 8. (a) Mean values of martensite block length (l_B), width (w_B) and aspect ratio (φ_{Block}) with respect to the PAGS. (b) Block length and width distributions. (c) Blocks aspect ratio distributions; (d) Evolution of retained austenite average grain size (d_{RA}) with the PAGS. (e–f) size and aspect ratio distribution (φ_{RA}) of the retained austenite. Dashed and solid lines are drawn as a guide for the eye.

microstructures are summarized in Table 2. As Table 2 shows, the Q&P microstructures created from PAGS of 6 and 67 μm are essentially free of fresh martensite. In the case of microstructure Q&P–185 μm, the domain size was defined based on the extrapolation of the trends in Fig. 8 and SEM observations, as indicated by a green arrow in Fig. 6. In addition, austenite features with sizes below the EBSD step size were considered in the simulations on the basis of experimental observations in the literature. As observed by transmission electron microscopy, thin films of austenite of 20–100 nm in thickness exist in between martensite laths of thickness of 0.2 μm independently of the PAGS [31,32]. The austenite morphology and distribution is schematically represented in Fig. 9b, where the presence of blocks and films of austenite is exemplified by IPF EBSD maps.

Fig. 10 displays the carbon profiles after different partitioning times for the different phase sizes. The α′/γ interface is located at the zero distance. The distribution of carbon occurs similarly in all cases. At low partitioning times ($t_P = 0.001$–0.01 s), the carbon content in the martensite next to the interface decreases readily below 0.01 wt% and a sharp spike of carbon appears in the austenite next to the interface. This spike diminishes and broadens with the increase of partitioning time, indicating that the carbon is diffusing within the austenite. A flat carbon profile develops in austenite films after 1 s of isothermal holding (Fig. 10a), whereas larger austenite blocks require longer times (Fig. 10b–e). The larger the austenite block, the longer the time required for carbon homogenisation.

The combined effect of carbon redistribution kinetics and microstructure dimensions on the stabilisation process of the austenite is discussed by comparing the microstructures Q&P–6 μm ($T_Q = 225$ °C) and Q&P–67 μm ($T_Q = 260$ °C). As Table 2 shows, these microstructures present similar phase fractions since the selected quenching temperatures allow the austenite to be completely stabilised, suppressing the formation of fresh martensite (Fig. 4). Therefore, it is assumed that the size and distribution of the phases at the beginning of the partitioning stage ($t_P = 0$ s) are comparable to those characterised in the final Q&P microstructures.

Fig. 10b shows that a homogeneous carbon profile in austenite is obtained after $t_P = 10$ s in the Q&P–6 μm microstructure. The carbon content across the austenite block is similar to that measured by XRD in the retained austenite. Assuming that the minimum carbon measured by XRD (0.85 ± 0.02 wt%) is the minimum required for stabilisation (indicated by the dotted line in Fig. 10a–d), this indicates that practically the total carbon fraction present in a martensite block is needed to stabilise an adjacent austenite grain. The small size and narrow distribution of phases in Q&P–6 μm (Fig. 8) makes the feature sizes used for the simulation representative of the entire microstructure. This leads to a good agreement between experiments and 1D simulations in this case. Instead, carbon homogenisation across the larger austenite blocks of the Q&P–67 μm microstructure (Fig. 10c) takes longer times and yields carbon contents well above the experimental value. This disagreement between experiments and simulations is attributed to the increase of the prior austenite grain size, which results in the development of martensite blocks within a broader distribution of sizes during the Q&P cycle, mainly, due to two effects. On the one hand, compared to small-grained austenitic microstructures, the formation of martensite from large PAGSs occurs in a broader variety of sizes within each austenite grain. In small PAGSs though, the multivariant formation of martensite is partially suppressed due to the mechanical stabilisation of the austenite [33–35]. Then, the first packet/block to form is the largest one and

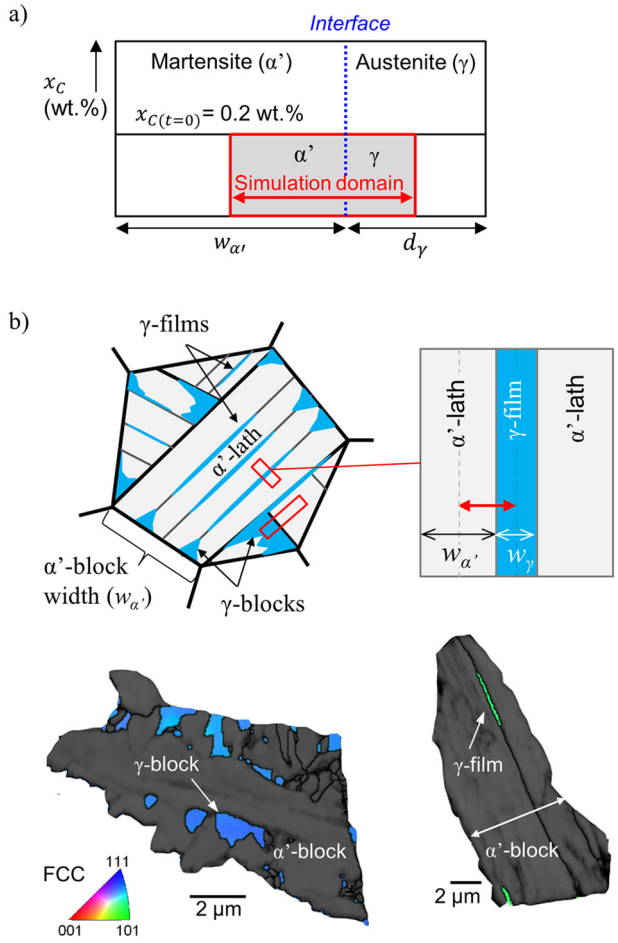

Fig. 9. (a) Schematic drawing of the simulation domain, where $w_{\alpha'}$ and d_γ stand for martensite block width and austenite grain size before partitioning. (b) Schematic illustration of the morphology and distribution of martensite and austenite and IPF EBSD maps of austenite exemplifying the presence of blocks and films of austenite.

grows predominantly, which results in mainly equiaxed martensite blocks within a narrower size distribution, as can be compared in Fig. 8b for Q&P–6 μm and microstructures with larger PAGSs. On the other hand, the increasing degree of skewness of the PAGS distribution as the PAGS is increased above 14 μm (Fig. 7) also contributes to the distribution broadening of the martensite blocks and untransformed austenite grains (Fig. 8b and e). This constituents size heterogeneity in Q&P–67 μm microstructure makes the redistribution of carbon during partitioning inhomogeneous, leading to a worse agreement between experiments and simulations compared to Q&P–6 μm microstructure.

In the case of the Q&P–185 μm microstructure, Fig. 10d shows that the complete homogenisation of carbon across austenite requires almost one hour of isothermal holding and results in a much lower carbon concentration than the minimum required for stabilisation. Instead, the carbon profiles developed after relatively short partitioning times lead to sufficient carbon enrichment of the first few hundred nanometres next to the α'/γ interface. Fig. 10e represents the carbon profiles (dashed lines) and fraction of retained austenite (solid lines) as a function of distance upon short (t_P = 50 s) and long (t_P = 3000 s) partitioning times. The local fraction of retained austenite at room temperature is calculated from the local austenite carbon concentration before the final quench. Upon short partitioning times, the fraction of stable austenite per grain increases as the partitioning time increases. However, due to the homogenisation process, there is a time above which the carbon profile decreases below the minimum content for stabilisation. This makes the fraction of retained austenite to recede, and after complete homogenisation the whole austenite grain transforms into fresh martensite. Similar observations were made by Mecozzi and co-authors [36], who applied a multiphase-field model to study the influence of the quench temperature on the retained austenite fraction for different partitioning conditions. Low quenching temperatures result in small austenite grains due to a further progress of the martensitic transformation. The carbon content within small austenite grains increases continuously with increasing partitioning times and so does the fraction of RA. However, when larger austenite grains originate from higher quenching temperatures, there is a partitioning time that optimizes the stabilisation of the austenite grain.

Size heterogeneity might be beneficial from the point of view of the mechanical properties as it allows austenite grains of different sizes to be stabilised with different carbon concentrations. This results in the retention of austenite with a gradient of stabilities, which provides sustained work-hardening rates through the transformation induced-plasticity effect extended to larger strains. However, it is difficult to control the degree of stability in austenite in this way and might result in the formation of undesirable fresh martensite. The present study shows an effect of the PAGSs similar to that observed by Mecozzi and co-authors [36]. Given similar fractions of primary martensite at the beginning of the partitioning stage, large untransformed austenite grains hamper the completion of the austenite stabilisation process. Therefore, for partitioning times of 50 s or less, the formation of fresh martensite is more likely to occur in the inner part of these large grains. In contrast, the small size and homogeneous distribution of phases in microstructures quenched from a PAGS of 6 μm makes it more efficient and easier to control the process of carbon partitioning.

4.2. Influence of the PAGS on the Q&P microstructural development

The complex microstructural processes involved in the development of Q&P steels cannot be completely described under the assumptions of full carbon partitioning, fixed interface and suppression of competitive reactions as proposed by Speer et al. [4]. It has been demonstrated that the martensite-austenite interface might be mobile under some conditions [11,12] and that the precipitation of carbides or austenite decomposition can often not be neglected [8–10]. Now, the present study demonstrates that the prior austenite grain size from which the Q&P microstructure develops, also plays a role in the stabilisation process of the

Table 2
Simulation phase sizes and experimentally measured phase fractions at the beginning of the partitioning step (t_P = 0 s) and in the final Q&P microstructure for different PAGSs and quenching temperatures. The first raw indicates the simulation domain size in the case of films of retained austenite, which are present in the microstructure regardless the PAGS and T_Q employed.

PAGS, μm	T_Q, °C	Phase sizes		t_P = 0 s		Final Q&P microstructure			
		$w_{\alpha'}$	d_γ^{unt}	f_{M1}	f_γ^{unt}	f_{M1}	f_B	f_{RA}	f_{M2}
	γ-films	0.20	0.05						
6	225	0.74	0.20	0.83	0.17	0.83	0.02	0.13	0.02
67	260	2.00	0.36	0.80	0.20	0.80	0.03	0.14	0.03
185	260	2.40	1.70	0.73	0.27	0.73	–	0.14	0.13
Error (±):				0.01	0.01	0.01	0.01	0.02	0.01

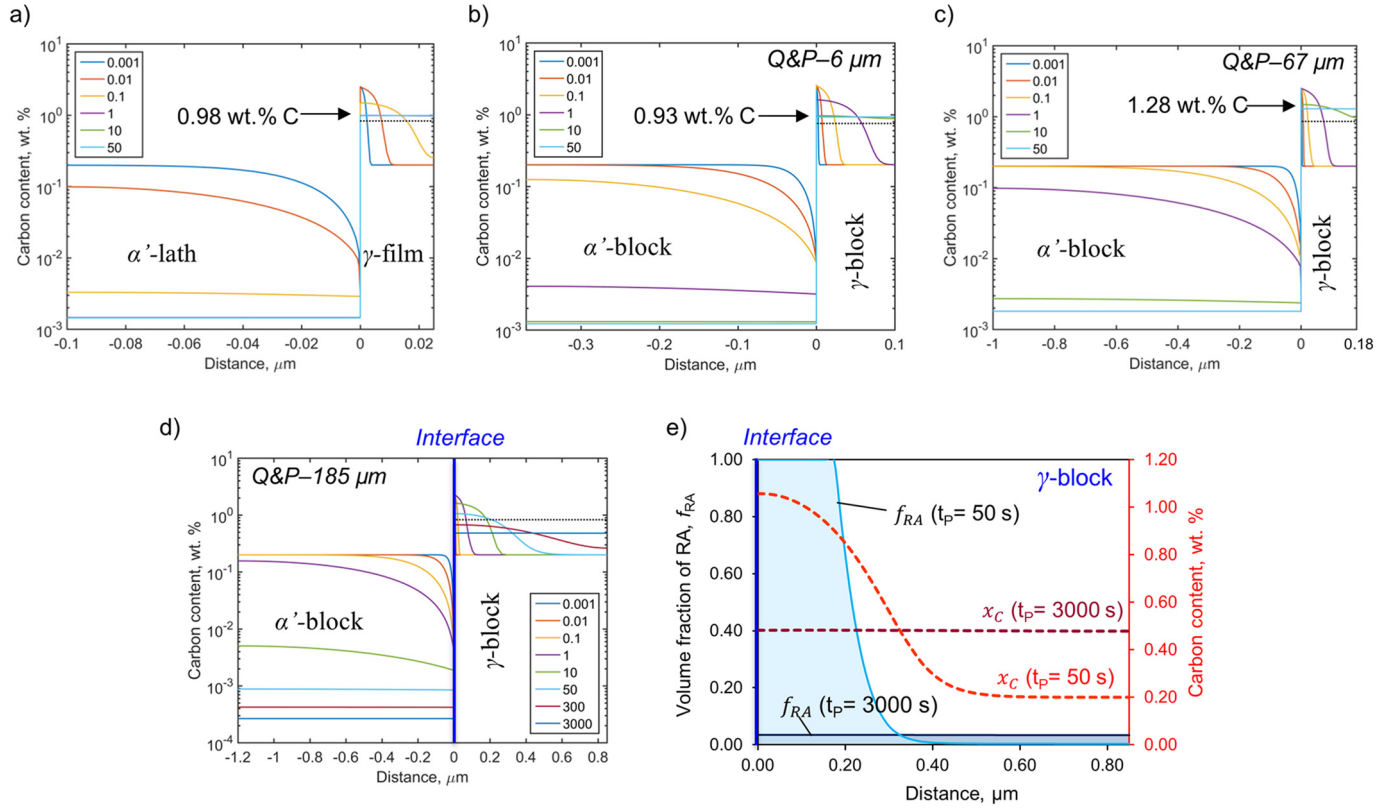

Fig. 10. (a–d) Carbon partitioning simulations for martensite (α′)/austenite (γ) of different sizes depending on the PAGS. The carbon content after complete homogenisation is noted; (e) Local volume fraction of RA (f_{RA}) corresponding to the carbon profiles across the γ-block in (d) after partitioning times of t_P=50 s and 3000 s.

austenite and influences the volume fraction, size and morphology of Q&P microconstituents. How these factors affect the final Q&P phase fractions and why is analysed in this section.

Fig. 2b showed that a microstructure with a small PAGS exhibits a lower M_S than a microstructure with a larger PAGS [16]. Therefore, by quenching to the same temperature, Q&P–6 μm microstructures

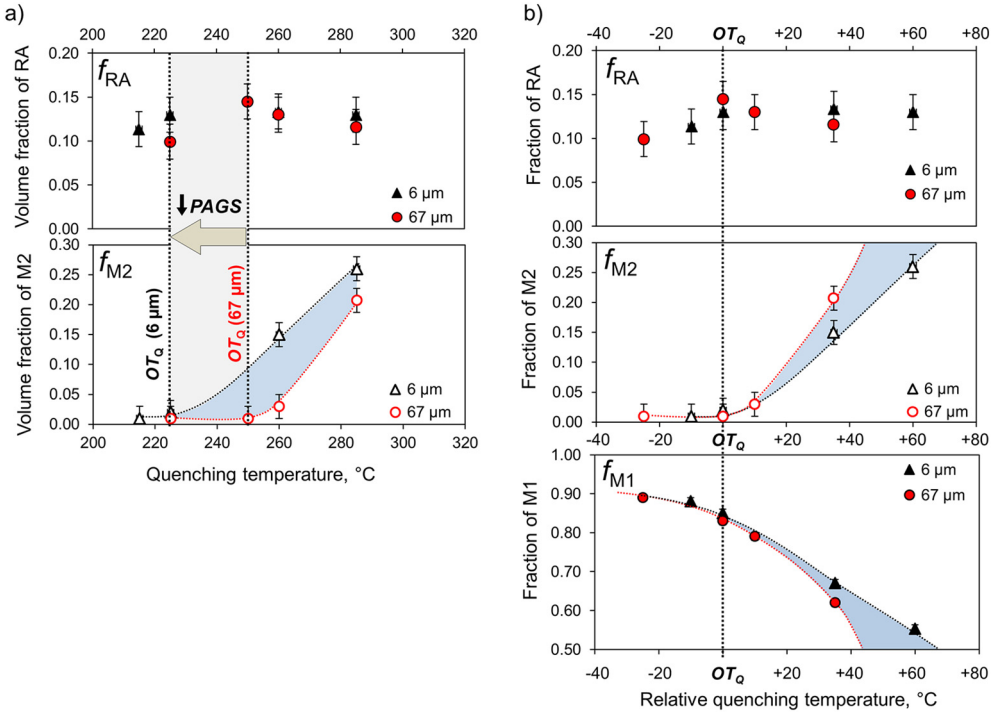

Fig. 11. Volume fraction of phases in microstructures created from PAGSs of 6 and 67 μm under similar Q&P conditions. In (a), the data are represented as a function of the quenching temperature. In (b), as a function of a relative quenching temperature that is selected to make the optimum quenching temperatures (OT_Q) of both PAGSs coincide. Dotted and dashed lines are drawn as a guide for the eye.

produce lower fractions of M1 than Q&P–67 μm and thus smaller fractions of carbon are available for the stabilisation of the austenite during the partitioning stage. Following the Q&P line of thought, under fixed quenching and partitioning conditions, larger fractions of fresh martensite would form with decreasing the PAGS.

Fig. 11a represents the measured phase fractions of retained austenite and fresh martensite as a function of the quenching temperature for microstructures Q&P–6 μm and Q&P–67 μm. The values of f_{RA} are quite insensitive to the quenching temperature. As experimentally demonstrated by Clarke and co-authors [37], partitioning times of 100 s or less at 400 °C lead to sufficient carbon enrichment in the austenite close to the interface enabling the retention of similar fractions of RA around the optimum quenching temperature (OT_Q). However, the incomplete homogenisation of carbon across the austenite grains might lead to the formation of M2 in the interior of austenite grains, as discussed in the previous section. The difference in M_S due to different PAGS creates a shift of comparable magnitude in the OT_Q (of around 30 °C) and same quenching temperatures result in higher fractions of M2 with decreasing PAGS, as highlighted in Fig. 11a by the blue shaded area. Thus, lower quenching temperatures are required to suppress the formation of M2 in Q&P–6 μm than in Q&P–67 μm microstructures. These results confirm the hypothesis made by Speer [14] about the possible effect of the PAGS on the prediction of Q&P phase fractions.

In order to unveil the real effect of the prior austenite structure on the Q&P microstructural development, the influence of the differences in M_S is eliminated by selecting a reference quenching temperature, for which the formation of fresh martensite is minimised and thus the optimum quenching temperatures of both PAGSs coincide in the figure (marked with dotted lines in Fig. 11a). Using this reference system, the evolution of phase fractions is plotted as a function of a relative quenching temperature in Fig. 11b. At the bottom of Fig. 11b, the evolution of volume fraction of M1 is added for comparison. Now, it is observed that higher fractions of M2 form in Q&P–67 μm than in Q&P–6 μm, which is attributed to the lower fractions of M1 obtained in the Q&P–67 μm microstructure resulting from a slower martensite formation kinetics. This evidences that, in addition to the effect of differences in M_S, variations in the martensite formation rate with the PAGS also influence the volume fraction of M1. As we have demonstrated in a previous study [16], once the martensitic transformation is initiated, the transformation rate in small-grained austenite is higher than that in coarser-grained microstructures. This originates from an increased nuclei density in the grain boundary area and from the development of elastic strain parallel to the martensite laths, which induces the repeated nucleation of more parallel martensite laths at the α'/γ interface in order to decrease the elastic strain energy. Although the influence of the martensite formation kinetics from different PAGSs on the final fraction of M2 is more pronounced for high quenching temperatures, it makes the Q&P microstructural development difficult to control based on processing parameters like the quenching temperature. Therefore, it is concluded that the thermal parameters should be adapted to design optimised Q&P microstructures from different PAGSs due to the effect of the austenite grain size on the M_S and on the martensitic transformation rate.

4.3. Enabling the design of Q&P microstructures from different PAGS

Originally, the design of Q&P microstructures has sought the retention of significant fractions of austenite as a way to increase the work hardening rate and to improve the mechanical behaviour in these steels [1]. Recent investigations have shown though, that the work hardening of the surrounding phases play an equally decisive role. For instance, the strength of the primary martensite can be engineered through controlled tempering to improve the ductility of martensite-austenite microstructures [38,39]. On the contrary, the hard fresh martensite is shown to negatively influence the austenite transformation stability due to its constraining effect on the strain distribution [17]. Thus, the interfaces between fresh martensite and a softer phase like primary martensite or retained austenite pose potential voids/cracks nucleation sites.

Fig. 11 shows that, upon the investigated partitioning conditions (400 °C, 50 s), the retention of the maximum fraction of austenite does not necessarily imply the suppression of fresh martensite. Additionally, the quenching temperature at which the M2 is suppressed depends on the PAGS (Fig. 11a). These facts indicate that the quenching temperature is not an adequate Q&P design parameter when the austenitisation conditions and, thus, the prior austenite grain size change.

Fig. 12 represents the evolution of the fraction and carbon content of RA (upper part) and the fraction of M2 (lower part) as a function of primary martensite fraction for all Q&P microstructures created from PAGSs in the range of 6 to 185 μm under the investigated partitioning conditions. It can be observed that, for the investigated partitioning conditions, the formation of a volume fraction of M1 of 0.77 or higher ensures the minimisation of M2 (f_{M2} of 0.07 or lower) and the retention of a maximum fraction of RA (f_{RA} in the range of 0.13–0.15) irrespective of the PAGS. The investigated partitioning conditions lead to the partitioning of all carbon to the surrounding austenite and the carbon diffuses similar distances irrespective of the grain size. Besides, the α′/γ interface remains immobile during the process of carbon diffusion and consequently the phase fractions remain unaltered during the partitioning step. For these reasons, the fraction of RA barely changes with the decrease of the fraction of M1 irrespective of the PAGS. As a consequence, the fraction of M2 varies linearly with M1 for low M1 fractions. The above mentioned phase fractions, which allow the RA the M2to be maximised and minimised, respectively, in the Q&P microstructure, offer a microstructural window (shaded area in Fig. 12) that allow an optimum fraction of primary martensite (Of_{M1}) to be defined. The formation of the optimum fraction of M1 for PAGSs of 6–67 μm leaves untransformed austenite with average grain sizes similar to or lower than twice the distance that carbon diffuses into austenite, as can be inferred from the carbon profiles in Fig. 10a–c. Flat carbon profiles develop after 50 s of partitioning, however, partitioning times as short as 10 s also result in sufficiently high carbon concentrations to

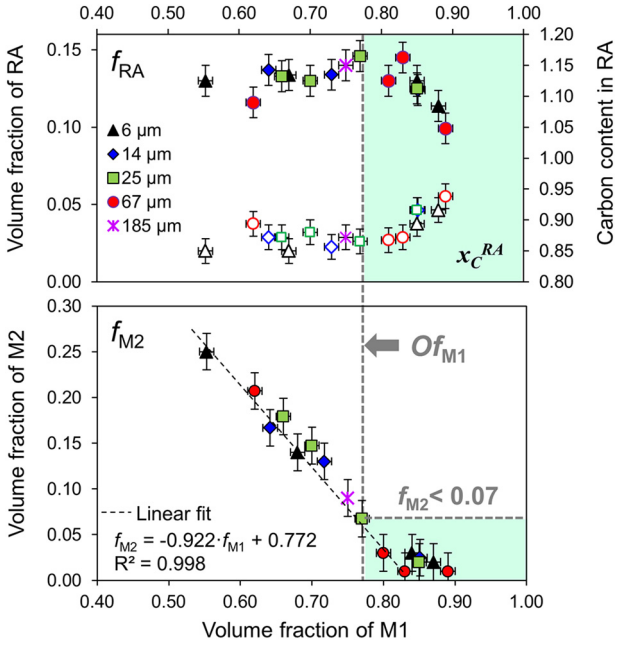

Fig. 12. Volume fraction and carbon content of RA (upper graph) and fraction of M2 (lower graph) as a function of the M1 fraction for Q&P microstructures created from PAGSs in the range of 6 to 185 μm. Shaded areas indicate simultaneous minimisation of M2 and maximisation of retained austenite. The optimum fraction of M1 (Of_{M1}) is represented by the dashed line.

stabilise the austenite. This ensures that the combination of the suggested optimum M1 fraction and the investigated partitioning conditions maximise austenite retention and minimise M2 formation in Q&P microstructures created from PAGSs of 6–67 μm. However, the optimum M1 fraction might show a dependency on the PAGS upon altered partitioning times. Due to the influence of a higher density of martensite/austenite interfaces, relatively short partitioning times stabilise larger austenite fractions in microstructures with small PAGSs than large PAGSs and, thus, less M2 should form. On the other hand, due to the more homogeneous spatial distribution and small size of phases, the carbon partitioning and homogenisation processes occur faster and more efficiently in microstructures with small PAGS. Thus, for M1 fractions lower than the optimum, relatively long partitioning times result in lower fractions of M2 compared to microstructures with larger PAGSs. In summary, upon short or long partitioning times, slight deviations in the optimum fraction of M1 to lower values could be expected in microstructures with small than with large PAGSs. The applied partitioning time of 50 s is seen to be in the intermediate range.

The optimum fraction of martensite is proposed as microstructural design parameter to eliminate the effect of the PAGS on the martensite formation kinetics during the first quench and, hence, to ensure the development of optimised Q&P microstructures. This new methodology can be successfully applied in the design of Q&P microstructures provided that the partitioning conditions ensure the partitioning of all carbon to the surrounding austenite. The optimum fraction of martensite proposed in this study applies for steels of similar composition that are fully austenitised, so that recrystallized austenite of grain size in the range of 6 μm to 185 μm is obtained. Significant modifications of the steel composition, especially in carbon content, or the pre-deformation of the prior austenite structure, as in direct quench and partitioning processing [40], will alter the martensite transformation kinetics during the first quench and the resulting size and morphology of the constituent phases. In these cases, a redesign of the optimum fraction of martensite is required. Additionally, it should be bear in mind that alteration of the partitioning conditions might affect the α'/γ interface mobility [11], the occurrence of competitive reactions [41] and, eventually, the final Q&P phase fractions. In these cases, the optimum fraction of M1 that maximises the stabilisation of austenite and minimises the formation of undesirable phases should be recalculated.

5. Conclusions

The influence of the prior austenite grain size (PAGS) on the quenching and partitioning (Q&P) microstructural development is investigated in a low carbon steel. The effect on the size and morphological aspects of the microconstituents is analysed in relationship with the kinetics of carbon redistribution between martensite and austenite upon fixed partitioning conditions of 400 °C and 50 s:

1) The thermal parameters to design Q&P microstructures should be tailored for different PAGSs since they result in different Q&P phase fractions. The PAGS influences the martensite start temperature (M_S) and the martensitic transformation rate during the first quench. On the one hand, the M_S is shifted to lower values with decreasing PAGS so that, when quenched to the same temperature, small-grained microstructures form smaller fractions of primary martensite than coarser microstructures. This provides a lower fraction of carbon for the stabilisation of austenite and eventually leads to the formation of higher fractions of fresh martensite. On the other hand, once the martensitic transformation is initiated, the transformation rate in small-grained austenite is higher than that in coarser-grained microstructures. Therefore, the adequate selection of Q&P thermal parameters for different PAGSs requires the accurate characterisation of the martensite formation kinetics; i.e. M_S and transformation rate.
2) Given similar fractions of primary martensite, small-grained austenitic microstructures (PAGS below 14 μm) result in a more efficient carbon partitioning process than coarser microstructures through the formation of smaller and more homogeneously distributed phases during the first quench. In contrast, the formation of martensite from larger PAGSs gives rise to microstructural heterogeneity. Size heterogeneity enables the stabilisation of austenite grains with a variety of sizes, carbon concentrations and thus stabilities. However, the degree of carbon enrichment in austenite during partitioning and thus the austenite stability is difficult to control in this way. Additionally, the formation of fresh martensite is more likely to occur in the interior of large grains of austenite due to the incomplete carbon homogenisation process.
3) In order to design Q&P microstructures considering the influence of the PAGS on the microstructural development an optimum microstructural parameter is proposed instead of the generally used optimum quenching temperature. An optimum fraction of primary martensite, which is independent of the PAGS, is defined to minimise the fraction of fresh martensite in the final microstructure and to stabilise a sufficient fraction of austenite. Under the partitioning conditions of 400 °C and 50 s, similar fractions of Q&P phases are obtained irrespective of the PAGS provided the formation of similar fractions of martensite during the first quench.

CRediT authorship contribution statement

Carola Celada-Casero: Conceptualization, Methodology, Validation, Formal analysis, Investigation, Writing - original draft, Visualization. **Cees Kwakernaak:** Data curation, Methodology, Software, Writing - review & editing. **Jilt Sietsma:** Writing - review & editing, Supervision, Project administration, Funding acquisition. **Maria Jesus Santofimia:** Conceptualization, Resources, Writing - review & editing, Supervision, Project administration, Funding acquisition.

Acknowledgments

The authors gratefully acknowledge the support from the Research Fund for Coaland Steel for funding this research under the Contract RFCS-02-2015 (Project No. 709755).

References

[1] D.K. Matlock, J.G. Speer, Third Generation of AHSS: Microstructure Design Concepts, Springer London, London, 2009 185–205.
[2] M.J. Santofimia, L. Zhao, R. Petrov, C. Kwakernaak, W.G. Sloof, J. Sietsma, Microstructural development during the quenching and partitioning process in a newly designed low-carbon steel, Acta Mater. 59 (2011) 6059–6068.
[3] M.J. Santofimia, L. Zhao, J. Sietsma, Microstructural evolution of a low-carbon steel during application of quenching and partitioning heat treatments after partial austenitization, Metall. Mater. Trans. A 40 (2008) 46.
[4] J. Speer, D.K. Matlock, B.C. De Cooman, J.G. Schroth, Carbon partitioning into austenite after martensite transformation, Acta Mater. 51 (2003) 2611–2622.
[5] J.G. Speer, F.C.R. Assunção, D.K. Matlock, D.V. Edmonds, The "quenching and partitioning" process: background and recent progress, Mater. Res. 8 (2005) 417–423.
[6] J.G. Speer, D.V. Edmonds, F.C. Rizzo, D.K. Matlock, Partitioning of carbon from supersaturated plates of ferrite, with application to steel processing and fundamentals of the bainite transformation, Curr. Opin. Solid State Mater. Sci. 8 (2004) 219–237.
[7] E.D. Moor, J.G. Speer, D.K. Matlock, J.-H. Kwak, S.-B. Lee, Effect of carbon and manganese on the quenching and partitioning response of CMnSi steels, ISIJ Int. 51 (2011) 137–144.
[8] Y. Toji, G. Miyamoto, D. Raabe, Carbon partitioning during quenching and partitioning heat treatment accompanied by carbide precipitation, Acta Mater. 86 (2015) 137–147.
[9] F. HajyAkbary, J. Sietsma, G. Miyamoto, T. Furuhara, M.J. Santofimia, Interaction of carbon partitioning, carbide precipitation and bainite formation during the Q&P process in a low C steel, Acta Mater. 104 (2016) 72–83.
[10] A.S. Nishikawa, M.J. Santofimia, J. Sietsma, H. Goldenstein, Influence of bainite reaction on the kinetics of carbon redistribution during the quenching and partitioning process, Acta Mater. 142 (2018) 142–151.
[11] M.J. Santofimia, J.G. Speer, A.J. Clarke, L. Zhao, J. Sietsma, Influence of interface mobility on the evolution of austenite–martensite grain assemblies during annealing, Acta Mater. 57 (2009) 4548–4557.

[12] M.J. Santofimia, L. Zhao, J. Sietsma, Model for the interaction between interface migration and carbon diffusion during annealing of martensite–austenite microstructures in steels, Scr. Mater. 59 (2008) 159–162.
[13] Cho L, Seo EJ, De Cooman BC. Near-Ac3 austenitized ultra-fine-grained quenching and partitioning (Q&P) steel. Scr. Mater. 2016;123:69–72.
[14] J.G. Speer, E. De Moor, A.J. Clarke, Critical assessment 7: quenching and partitioning, Mater. Sci. Technol. 31 (2015) 3–9.
[15] R.A. Grange, The rapid heat treatment of steel, Metall. Trans. A. 2 (1971) 65–78.
[16] C. Celada-Casero, J. Sietsma, M.J. Santofimia, The role of the austenite grain size in the martensitic transformation in low carbon steels, Mater. Des. (2019) 107625.
[17] D. De Knijf, R. Petrov, C. Föjer, L.A.I. Kestens, Effect of fresh martensite on the stability of retained austenite in quenching and partitioning steel, Mater. Sci. Eng. A 615 (2014) 107–115.
[18] S. Morito, X. Huang, T. Furuhara, T. Maki, N. Hansen, The morphology and crystallography of lath martensite in alloy steels, Acta Mater. 54 (2006) 5323–5331.
[19] C.F. Jatczak, Retained austenite and its measurement by X-ray diffraction, SAE Int. 89 (1980) 1657–2676.
[20] J.B. Nelson, D.P. Riley, An experimental investigation of extrapolation methods in the derivation of accurate unit-cell dimensions of crystals, Proc. Phys. Soc. 57 (1945) 160–177.
[21] N.H. van Dijk, A.M. Butt, L. Zhao, J. Sietsma, S.E. Offerman, J.P. Wright, et al., Thermal stability of retained austenite in TRIP steels studied by synchrotron X-ray diffraction during cooling, Acta Mater. 53 (2005) 5439–5447.
[22] S.M.C. van Bohemen, The nonlinear lattice expansion of iron alloys in the range 100–1600 K, Scr. Mater. 69 (2013) 315–318.
[23] M.J. Santofimia, L. Zhao, J. Sietsma, Volume change associated to carbon partitioning from martensite to austenite, Mater. Sci. Forum 706-709 (2012) 2290–2295.
[24] M.J. Santofimia, R.H. Petrov, L. Zhao, J. Sietsma, Microstructural analysis of martensite constituents in quenching and partitioning steels, Mater. Charact. 92 (2014) 91–95.
[25] S. Morito, H. Tanaka, R. Konishi, T. Furuhara, T. Maki, The morphology and crystallography of lath martensite in Fe-C alloys, Acta Mater. 51 (2003) 1789–1799.
[26] S.M.C. van Bohemen, L. Morsdorf, Predicting the Ms temperature of steels with a thermodynamic based model including the effect of the prior austenite grain size, Acta Mater. 125 (2017) 401–415.
[27] C.C. Kinney, K.R. Pytlewski, A.G. Khachaturyan, J.W. Morris Jr., The microstructure of lath martensite in quenched 9Ni steel, Acta Mater. 69 (2014) 372–385.
[28] J. Hidalgo, M.J. Santofimia, Effect of prior austenite grain size refinement by thermal cycling on the microstructural features of as-quenched lath martensite, Metall. Mater. Trans. A (2016) 1–14.
[29] C.A. Apple, R.N. Caron, G. Krauss, Packet microstructure in Fe-0.2 pct C martensite, Metall. Trans. A. 5 (1974) 593–599.
[30] T. Swarr, G. Krauss, The effect of structure on the deformation of as-quenched and tempered martensite in an Fe-0.2 pct C alloy, Metall. Trans. A. 7 (1976) 41–48.
[31] C.Y. Wang, J. Shi, W.Q. Cao, H. Dong, Characterization of microstructure obtained by quenching and partitioning process in low alloy martensitic steel, Mater. Sci. Eng. A 527 (2010) 3442–3449.
[32] X.C. Xiong, B. Chen, M.X. Huang, J.F. Wang, L. Wang, The effect of morphology on the stability of retained austenite in a quenched and partitioned steel, Scr. Mater. 68 (2013) 321–324.
[33] S. Takaki, K. Fukunaga, J. Syarif, T. Tsuchiyama, Effect of grain refinement on thermal stability of metastable austenitic steel, Mater. Trans. 45 (2004) 2245–2251.
[34] T. Furuhara, K. Kikumoto, H. Saito, T. Sekine, T. Ogawa, S. Morito, et al., Phase transformation from fine-grained austenite, ISIJ Int. 48 (2008) 1038–1045.
[35] S. Morito, H. Saito, T. Ogawa, T. Furuhara, T. Maki, Effect of austenite grain size on the morphology and crystallography of lath martensite in low carbon steels, ISIJ Int. 45 (2005) 91–94.
[36] M.G. Mecozzi, J. Eiken, M.J. Santofimia, J. Sietsma, Phase field modelling of microstructural evolution during the quenching and partitioning treatment in low-alloy steels, Comput. Mater. Sci. 112 (Part A) (2016) 245–256.
[37] A.J. Clarke, J.G. Speer, D.K. Matlock, F.C. Rizzo, D.V. Edmonds, M.J. Santofimia, Influence of carbon partitioning kinetics on final austenite fraction during quenching and partitioning, Scr. Mater. 61 (2009) 149–152.
[38] K.O. Findley, J. Hidalgo, R.M. Huizenga, M.J. Santofimia, Controlling the work hardening of martensite to increase the strength/ductility balance in quenched and partitioned steels, Mater. Des. 117 (2017) 248–256.
[39] J. Hidalgo, K.O. Findley, M.J. Santofimia, Thermal and mechanical stability of retained austenite surrounded by martensite with different degrees of tempering, Mater. Sci. Eng. A 690 (2017) 337–347.
[40] M.C. Somani, D.A. Porter, L.P. Karjalainen, P.P. Suikkanen, R.D.K. Misra, Process design for tough ductile martensitic steels through direct quenching and partitioning, Mater. Today 2 (2015), S631-S4.
[41] J. Hidalgo, C. Celada-Casero, M.J. Santofimia, Fracture mechanisms and microstructure in a medium Mn quenching and partitioning steel exhibiting macrosegregation, Mater. Sci. Eng. A 754 (2019) 766–777.